Improved performance of quantum dots sensitized solar cells: a TiO_2-nano-SiO_2 hybrid photoanode modified with CdSe

RENBAO WANG[a], HUI ZHANG[a], QIONG MA[b], HAIHONG NIU[b], JINZHANG XU[b]
[a]*Department ElectronicInformation and Electrical Engineering, Hefei University, Hefei 230601, China*
[b]*School of Electrical Engineering and Automation, Hefei University of Technology, Hefei 230009, China*

A new type of TiO_2-nano-SiO_2 hybrid film was prepared by mixing TiO_2 with the nano-sized SiO_2 powder. The size of CdSe quantum dots (QDs) was about 2.6nm. The spin-coating method was applied to prepare CdSe QDs sensitized the TiO_2-nano-SiO_2 hybrid film for the quantum dots sensitized solar cells (QDSSCs) application. It is found that the introduction of SiO_2 and the capped ligands show notable influence on the photovoltaic performance. The power conversion efficiency of 1.74% was achieved by using the TiO_2-nano-SiO_2 hybrid film modified with MPA-capped CdSe (TiO_2-nano-SiO_2/CdSe(MPA)) under the illumination of one sun (AM1.5, 100mW/cm^2).

(Received February 3, 2019; accepted February 17, 2020)

Keywords: CdSe quantum dots, TiO_2-nano-SiO_2 hybrid photoanode, Sensitized, Solar cells

1. Introduction

Since the sandwich architecture for the dye-sensitized solar cells (DSSCs) was developed by Grätzel in 1991 [1], it has drawn much attention [2, 3]. Up to now, the highest efficiency of DSSCs reached over 20% [4]. QDs can also serve as solar cells sensitization [5, 6] because they can transfer electrons to large band gap semiconductors. QDSSCs have been attracting much attention because of the specific advantages of QDs. First, size quantization effect allows one to tune the visible response and vary the band energies to modulate the vectorial charge transfer across different-sized particles [7]. In addition, QDs can generate multiple excitons carriers with a single photon through impact ionization [8]. Recently, sensitization of mesoporous metal oxide layers (such as TiO_2, ZnO, SnO_2) with QDs (such as CdS [9, 10, 11], CdPbS [12], CdSe [13, 14], InP [15], InAs [16], Bi_2S_3 [17], PbS [18]) were proposed. Other materials (such as Ag@Cu_2O core-shell nanoparticles [19], nitrogen-doped lanthanum titanium oxides [20], hematite/reduced graphene oxide composites [21], nickel oxide-hematite p-n junction [22]) were also utilized for solar energy application. The nanocrystalline TiO_2 film has interconnected mesoporous structure featured with the large surface area which offers an increased adsorption amount of QDs. But the charge recombination between electrons and electrolytes will inevitably take place owing to exposure of surface sites to electrolytes on semiconductor. Therefore, the power conversion efficiency of QDSSCs is still far from satisfactory.

To retard interfacial recombination, SiO_2/TiO_2 composite powders are used as the semiconductor substance of the hybrid electrode, which are prepared by adding the nano-sized SiO_2 into the TiO_2 in the paper. The introduction of SiO_2 is crucial to decrease agglomeration and enhance dispersion of TiO_2, which helped to achieve the better connection and the higher electron transfer efficiency at TiO_2/CdSe interfaces and internal TiO_2 grain boundaries. And SiO_2 is a wide band-gap (8~9eV) material which offers an insulated layer between the photo-excited electrons and the electrolyte. Thus, the charge recombination between semiconductor and electrolyte is reduced. Simultaneously, MPA that has a shorter alkyl chain is utilized to replace the long chain TDPA, which minimizes the interparticle spacing to promote charge transport and lowers the defect density to reduce charge recombination loss. MPA has a hydrophilic group, MPA-capped CdSe QDs can be dissolved in the aqueous solvent. Thus, the material is green and cheap. The TiO_2-nano-SiO_2 hybrid film is modified with MPA-capped CdSe QDs through the spin-coating method, which makes the simple assembly route of CdSe-QDSSCs photoanodes. The conclusion is drawn that the ligand exchange and the incorporation of nano-sized SiO_2 can improve the photovoltaic performance of QDSSCs. The TiO_2-nano-SiO_2/CdSe(MPA) photoanode exhibited the power conversion efficiency of 1.74%.

2. Experimental

2.1. Preparation of TiO_2-nano-SiO_2 hybrid photoanode

The paste was made as follows [23]. Firstly, TiO_2 (10g, Degussa) mixed with SiO_2 (0.5g, Degussa) was grinded for 5min. Acetic acid (3ml), water (12ml), and ethanol (50ml) were subsequently added to the powder and grinded for 10min. Secondly, the grinded paste was diluted with ethanol (200ml), and stirred for 1h, followed by ultrasonic treatment for 1h. Thirdly, the paste was mixed with terpineol (40g), ethanol (60g), and ethyl cellulose (6g), respectively. The mixture was homogenized by stirring and ultrasonic treatment. Finally, ethanol was evaporated by the rotary-evaporator at 45℃. The cleaned F-doped tin oxide (FTO, 20V/A) coated glass substrates were immersed into an aqueous solution of $TiCl_4$ (0.1 M), and dried in an airflow at 80℃ for 30min. A layer of film was fabricated on the FTO surface by screen-printing method. Then, the TiO_2-nano-SiO_2 hybrid film was obtained after annealed at 500℃ for 30min.

The TiO_2 film was obtained using the similar approach. The TiO_2-nano-SiO_2 hybrid film and the TiO_2 film were clean and dry after annealed. The two types of film were scraped with the blade gently, and were ground carefully. N_2 was adsorptive, and two types of ground film were adsorbent. At the standard temperature and pressure (STP), the physical adsorption experiments of two types of nano-porous film were tested by the N_2 adsorption-desorption analyzer (Tristar II 3020 M). Thus, the N_2 adsorption-desorption isotherms and pore-size distribution profiles of TiO_2 powders and TiO_2-nano-SiO_2 powders were obtained.

CdSe QDs were prepared according to the method with few modifications [24]. CdO (50mg, Aldrich), TOPO (2000mg, Aldrich), and TDPA (300mg, Aldrich) were degassed at 110ºC for 70min and then heat under nitrogen to 300ºC to completely dissolve the precursors. TOPSe (18mg of Se (Aldrich) dissolved in 4.0mL of TOP (Aldrich)) was quickly injected into the reaction vessel to initiate the reaction. After 2min of growth at 280℃, the resulting solution was cooled to room temperature, and the CdSe QDs were precipitated with isopropanol, methanol and toluene, and dissolved in toluene for use.

About 0.2g of MPA was dissolved in 10ml of methanol, and its pH value was controlled at 11 to 12 through dropping the saturated methanol solution of sodium hydroxide. The aforesaid solution (~12ml) was added to the toluene solution of TDPA-capped CdSe (~12ml), then stirred for 10min and centrifuged for 10min. The resulting precipitation was dissolved in 12ml of water for use. Such, CdSe QDs underwent ligand exchange with MPA.

The adsorption behavior of CdSe QDs with two kinds of ligands was studied. (1) CdSe QDs were initially prepared with their surface surrounded by TDPA. (2) TDPA ligand was replaced with MPA. TDPA-surrounded CdSe QDs were added into TiO_2-nano-SiO_2 films using the spin-coating method. The spin-coating steps were at 3,000 r.p.m. Each iteration had two steps: (1) three drops of CdSe QDs solution was dropped onto a static TiO_2-nano-SiO_2 substrate and spun for 25s; (2) the film was flushed with the toluene and then spun (~10s) to dry the film. The sensitized photoanode was gotten after the procedure was repeated ~5 times. Finally the photoanode was covered with the ZnS layer by alternate dipping into solutions of $Zn(NO_3)_2$ (0.1M) and Na_2S (0.1M) [25]. The MPA-surrounded CdSe QDs was fabricated using the similar approach. The spin-coating method was advantages to saving materials and time. The MPA-surrounded CdSe QDs dissolved in water were anchored in big quantities over TiO_2-nano-SiO_2 layers, as could be seen from a crimson change in color after the sensitization process. In contrast, The TDPA-surrounded CdSe QDs dissolved in toluene had a pale change in color. The phenomenon might illuminated that the adsorption behavior of CdSe was sensitive to experimental conditions such as the choice of solvent for CdSe dispersion, and the ligands used in the preparation.

2.2. Fabrication and measurement of QDSSCs

The CdSe-modified TiO_2-nano-SiO_2 electrode was incorporated as the active photoanode. The Pt coated FTO conductive glass was used as the counter electrode. The two electrodes were sandwiched by thermal adhesive film (Surlyn1702, Dupont). The electrolyte solution consisted of Na_2S (0.5M), S (0.8M), and KCl (0.2M) [26]. The electrolyte was filled through a hole made on the counter electrode [27]. Photocurrent–voltage (J-V) measurement was performed with the solar simulator (94063A, Newport), equipped with the 1000W xenon lamp (6272NS, Newport) and the Keithley digital source meter (2400, USA). The QTest Station 1000 ADI system (Crowntech Inc.) illuminated with a 300W Xe was used during the measurements of incident photon to current conversion efficiency (IPCE).

3. Results and discussion

3.1. Characterization of CdSe-QDSSCs photoanodes

Fig. 1 shows the XRD patterns of annealed TiO_2 powders and TiO_2-nano-SiO_2 composite powders. It is seen that almost all diffraction peaks are assigned to anatase TiO_2 (JCPDS No. 84-1285) [28]. Diffraction peaks of rutile TiO_2 crystalline phase are not observed. It suggests that all the TiO_2 transform into anatase after treatment at 500ºC. SiO_2 crystalline phase isnot found, which demonstrates that the SiO_2 exists in its amorphous phase.

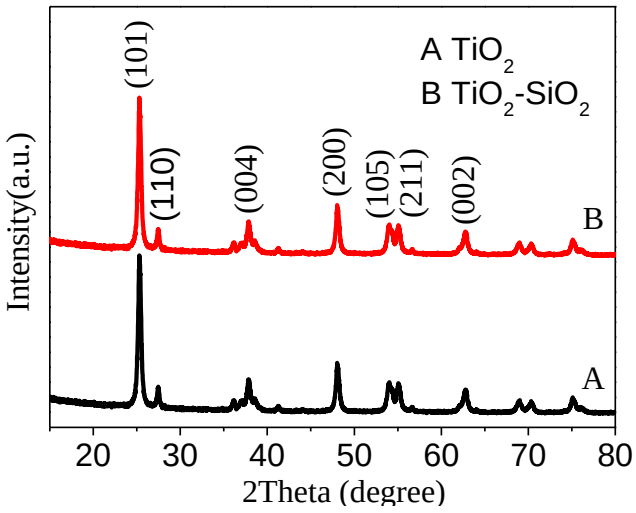

Fig. 1. XRD pattern of TiO_2 powders and TiO_2-nano-SiO_2 composite powders

The morphology and microstructure of films were studied by the scanning electron microscopy (SEM) and transmission electron microscopy (TEM) observation. Fig. 2 (A,B) displays the SEM images of TiO_2 and TiO_2-nano-SiO_2 composite layers on FTO substrate. It reveals that the two films share a porous structure, which is formed by the stack of TiO_2 particles. By statistically calculation, we find that the TiO_2-nano-SiO_2 composite film (Fig. 2B) has a higher pore density as compared to the TiO_2 film (Fig. 2A). A rational explanation is that the incorporation of nano-SiO_2 leads to higher dispersion of TiO_2 nanoparticles, which causes smaller pores in the TiO_2-based thin film. Fig. 2(C, D) shows the TEM images of nanoparticles. TiO_2 nanparticles, which are quasi-sphere shapes, are in connection each other, and form a network. After introduction of SiO_2, the crystallite shapes are not significantly changed. Fig. 2E shows a typical SEM cross section, and a hybrid film with ~14μm. Fig. 2F shows the high-resolution transmission electron microscopy (HR-TEM) image of nanoparticle. The lattice fringes are clear, which indicates that the nanoparticle is a single crystal of anatase TiO_2. The lattice distance is in consistent with (101) plane of the anatase phase [29]. The results agree well with XRD analysis. The films are further characterized by N_2 adsorption-desorption (Fig. 2G, 2H). The shapes of isotherms are typical of meso-porous materials [30]. The isotherm of TiO_2-nano-SiO_2 indicates that position of hysteresis loops gradually increases in comparison with that of TiO_2, which suggests that specific surface area increases and pore size decreases after SiO_2 is incorporated. The results are summarized in Table 1. It is found that the hybrid film has larger surface area and pore volume than the TiO_2 film. The surface area increased from 44.62m^2/g to 58.83m^2/g. The particle size is calculated according to the equation [31]:

$$d_{BET} = 6/(\rho_{TiO_2} \times S_{BET}), \rho = 3.9 g/cm^3$$

The distribution curves of pore size display a wide range of 2~90nm. The TiO_2-nano-SiO_2 film has a smaller average pore size as compared to the TiO_2 film. The reason is that the incorporation of nano-SiO_2 leads to better dispersion of TiO_2 nanoparticles, thus, generates more micro/meso-pores in TiO_2-based thin film, which results in higher surface area.

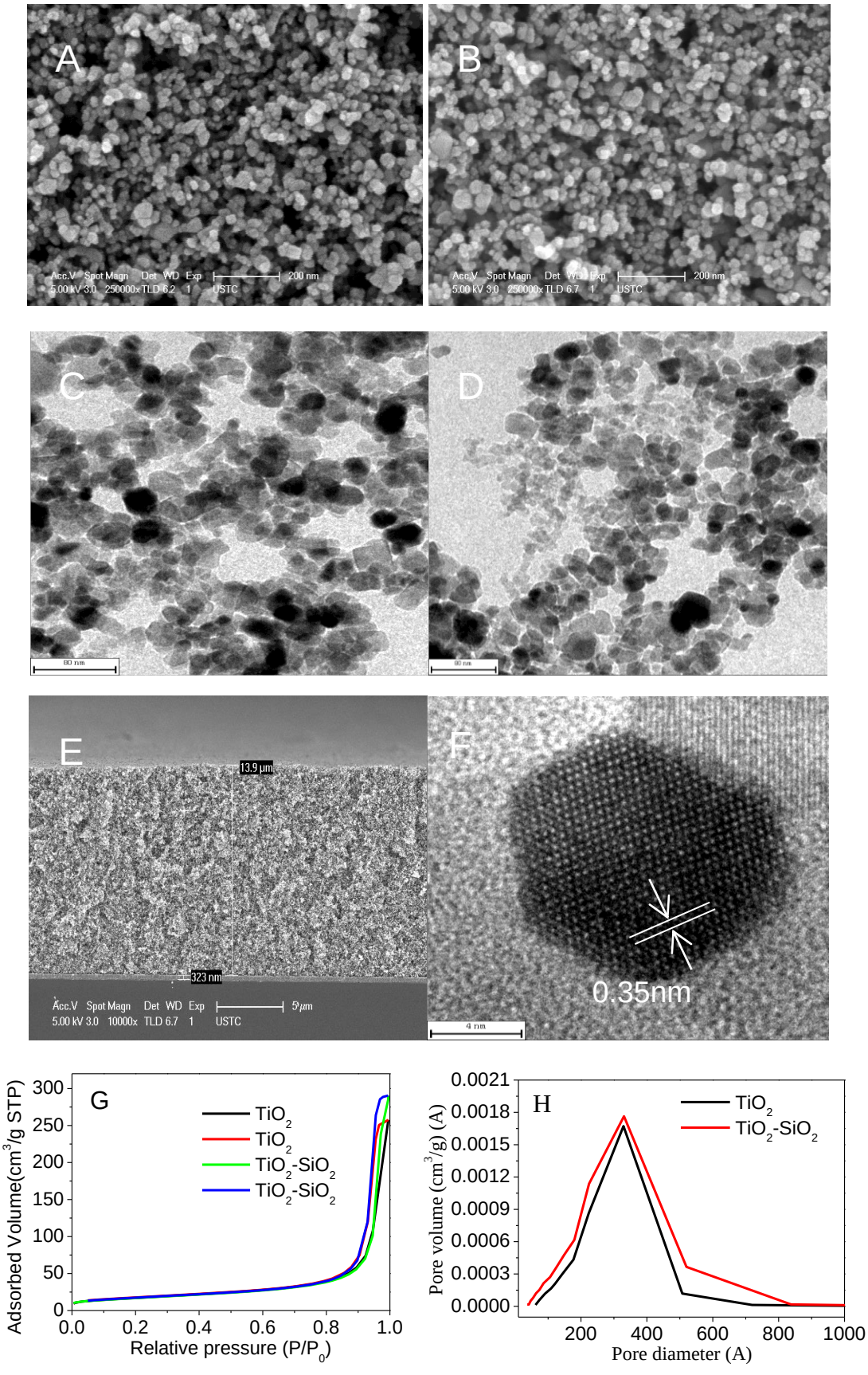

Fig. 2. SEM image (A) and TEM image (C) of TiO_2 film; SEM image (B), TEM image (D), and SEM cross section image (E) of TiO_2-nano-SiO_2 film; HR-TEM image of TiO_2 (F); N_2 adsorption-desorption isotherms (G) and pore-size distribution profiles (H) of TiO_2 powders and TiO_2-nano-SiO_2 powders (color online)

Table 1. The physical properties of the prepared hybrid films

Sample	BET (m^2/g)	Pore volume[a] (cm^3/g)	Pore size[b] (nm)	Porosity[c] (%)	Particle size (nm)
TiO_2	44.62	0.38	34.96	60.33	34.48
TiO_2-nano-SiO_2	58.83	0.44	29.91	63.18	26.15

[a]*Single point adsorption total pore volume*
[b]*Adsorption average pore width (4V/A by BET)*
[c]*Based on pore volume and 3.9g/cm^3 of anatase density*

The absorption and photoluminescence properties of CdSe QDs dispersed in toluene is displayed in Fig. 3(A). CdSe QDs exhibite typical absorption characteristics (a sharp excitonic peak at 546nm). By the empirical equations, the diameter of CdSe QDs is estimated to be ~2.6nm [32, 33]. TEM image of CdSe nanoparticles is showed in Fig. 3(B). Clearly, nearly monodisperse and high-quality semiconductor CdSe nanocrystals are obtained by the method.

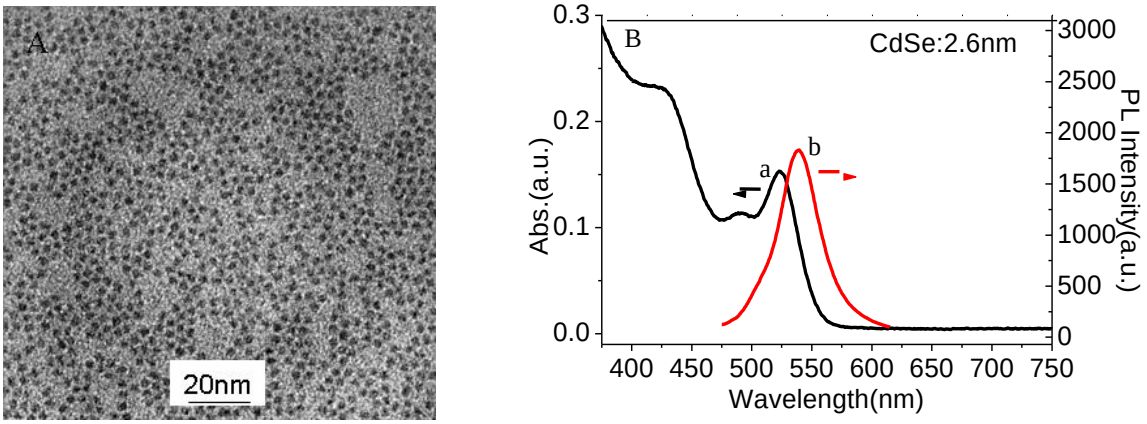

Fig. 3. TEM image (A), and absorption and emission spectra (B) of CdSe nanocrystals suspension in toluene. The excitation wavelength is 365nm (color online)

The AFM images of CdSe QDs linked to TiO_2-nano-SiO_2 films were shown in Fig. 4. The morphology is apparent from the surface topography. TiO_2-nano-SiO_2 film provides the necessary foundation for anchoring CdSe QDs via molecular linkers. The morphology of the TiO_2-nano-SiO_2 film becomes rougher after assembling of CdSe. Furthermore, the mesoscopic morphology of the TiO_2-nano-SiO_2 film facilitates penetration of CdSe QDs through pores in the matrix, enabling their uniform binding to both interior and exterior TiO_2-nano-SiO_2 film surfaces.

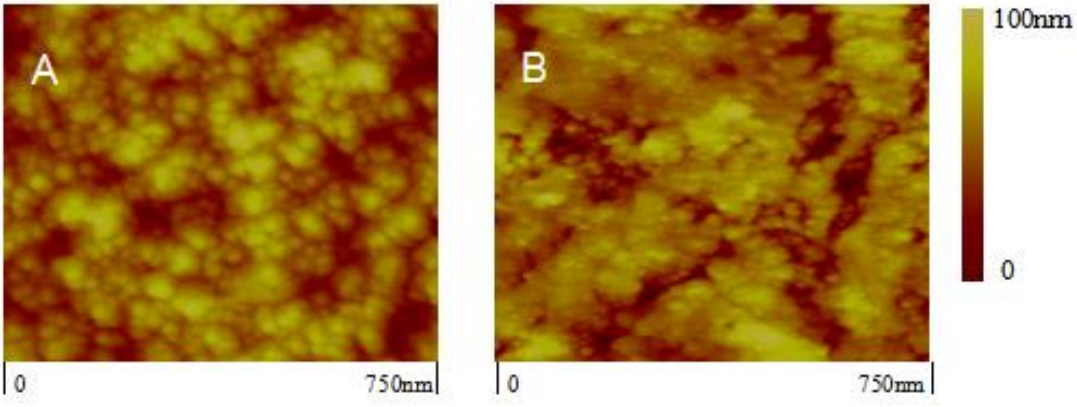

Fig. 4. AFM images of a TiO_2-nano-SiO_2 film (A), and the film after introduction of CdSe (B) (color online)

UV-vis absorption spectra, recorded after linking CdSe QDs to films with different ligands, are shown in

Fig. 5. The absorption edges, obtained from the intersection of the sharply decreasing region of a spectrum with its baseline, are ~600nm for all the electrodes. The absorbance of TiO_2-nano-SiO_2/CdSe(MPA) electrode is highest among the photoanodes, which implies that more CdSe QDs is loaded on the electrode. The result also indicates that the deposition rate of CdSe on the TiO_2-nano-SiO_2 film is better than on the TiO_2. However, the absorbance of TiO_2/CdSe(TDPA) is lowest among the electrodes, ascribed to the lowest amount of TDPA-capped CdSe assembled on the TiO_2. The reason for the increased absorbance is that the larger number of binding sites can be available for MPA-capped CdSe QDs within TiO_2-nano-SiO_2 films. MPA linker provides better coverage of CdSe QDs on TiO_2-nano-SiO_2 films, suggesting that short chain linker is better suited for this purpose.

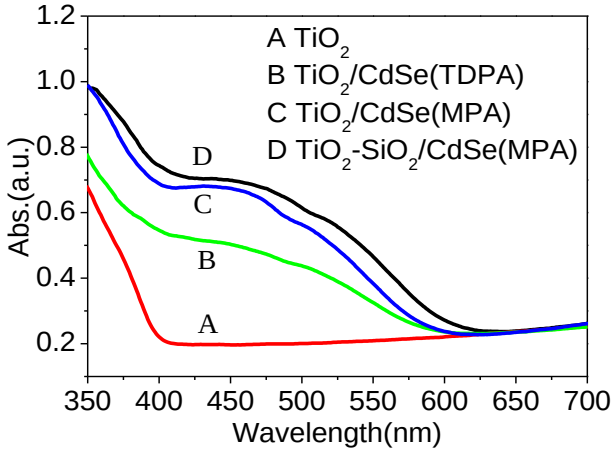

Fig. 5. UV-vis absorption spectra of TiO_2 film and TiO_2-nano-SiO_2 films sensitized by CdSe QDs (color online)

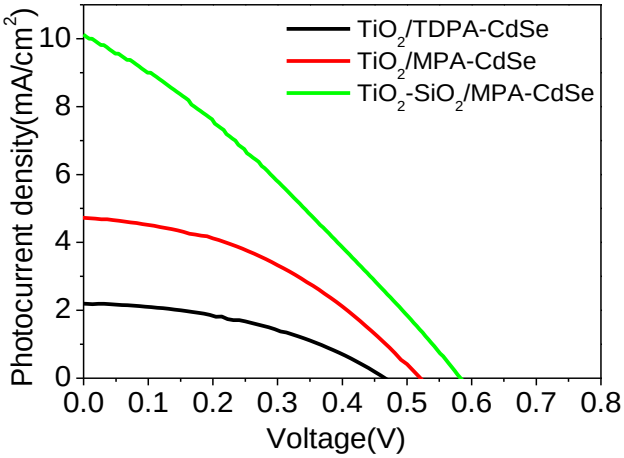

Fig. 6. J-V characteristics of QDSSCs using various photoanodes (color online)

3.2. Characterization of CdSe-QDSSCs

To study the photovoltaic performance, we fabricate the standard QDSSCs using the TiO_2-nano-SiO_2 hybrid films as photoanodes. Fig. 6 presents the J–V characteristics of the fabricated solar cells, and the parameters from J–V curves were described in Table 2.

Table 2. Parameters obtained from the J-V profiles of QDSSCs using various electrodes

Electrode	Open-circuit Voltage (V_{oc}) (V)	Short-circuit Current Density (J_{sc}) (mA/cm^2)	Fill Factor (FF)	η (%)
TiO_2/CdSe(TDPA)	0.46	2.2	0.44	0.45
TiO_2/CdSe(MPA)	0.52	4.7	0.41	0.98
TiO_2-nano-SiO_2/CdSe(MPA)	0.58	10.1	0.31	1.74

The most notable variation is the short-circuit current (J_{sc}) density and the power conversion efficiency (η). For the TiO_2/CdSe(MPA) device, the power conversion efficiency is 0.98%, which is higher than the TiO_2/CdSe(TDPA) device. The increment of J_{sc} from 2.2 to 4.7mA/cm^2 is achieved. The result indicates that MPA-capped CdSe QDSSCs can lead to a significant efficiency increase. The reason is that MPA has a shorter alkyl chain, and thus the interparticle spacing is minimized to promote charge transport, and the defect density is lowered to reduce charge recombination loss.

The maximum power conversion efficiency is 1.74% for TiO_2-nano-SiO_2 film modified with MPA-capped CdSe QDs, and the corresponding J_{sc} is 10.1mA/cm^2. It is evident that introduction of SiO_2 can enhance the efficiency and current density of QDSSCs. The high current density is due to the improvement in the light harvesting capacity of the photoanode. The first reason is the more micro/meso-pores and the larger pore volume in the hybrid film, which is seen from the Table 1. The electrical contact among nanoparticles is improved, thus, the charge transport is rectified. The second reason is that SiO_2 has a wide band-gap, and works as a partial barrier layer in the phtoanode. Thus, the recombination of electron in TiO_2 porous film and S^{2-}/S_n^{2-} in electrolyte is prevented.

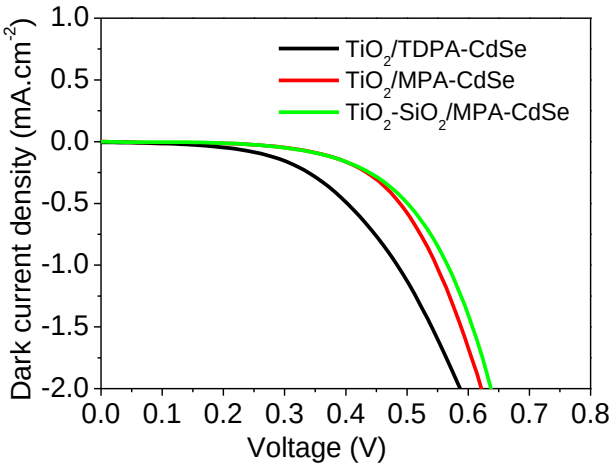

Fig. 7. Dark current under the conditions of dark (color online)

Fig. 7 showed the dark-current−voltage curve of the QDSSCs measured under bias potential (-0.5V). The dark-current onset of TiO_2/CdSe(TDPA) photoanode occurred at low forward bias, indicating faster electron-recombination kinetics. TiO_2-nano-SiO_2/CdSe(MPA) photoanode gradually shifts the dark-current onset to the higher forward bias. It can be attributed that the minimized direct contact between semiconductor and electrolyte. The introduction of SiO_2 probably passivated the reactive sub-band-edge surface-states. Thus, the conclusion was draw that the SiO_2 is important to electron transport and light scattering, ultimately obtaining the higher power conversion efficiency.

The IPCE profiles are given in Fig. 8, which resemble the absorption spectra of CdSe QDs reasonably well (Fig. 5). All the solar cells show photocurrent responses below 600 nm. A maximum IPCE value of 28% is observed for the TiO_2/CdSe(MPA) device. IPCE values of CdSe/TiO_2 films prepared using TDPA linker molecule show lower efficiencies with a maximum IPCE value of 15%. The lower IPCE values imply that a larger number of carriers are lost to charge recombination at the CdSe/TiO_2 interface or within the particles. Thus, MPA is better than TDPA as the linker for anchoring CdSe QDs to TiO_2. The maximum IPCE value as high as 40% can be obtained at maximum peak for the TiO_2-nano-SiO_2/CdSe(MPA) device. The results show that the introduction of SiO_2 further increases the IPCE value.

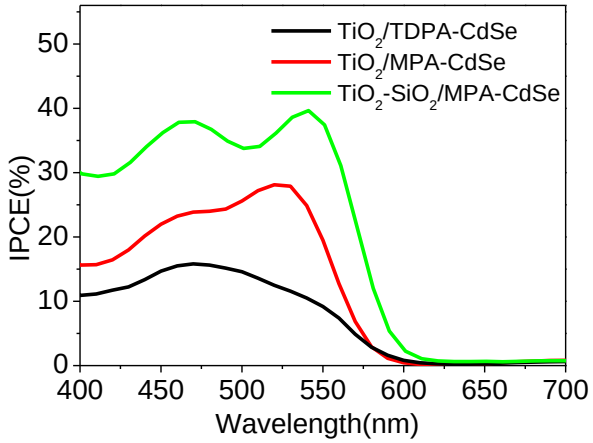

Fig. 8. IPCE spectra of QDSSCs using various photoanodes (color online)

Electrochemical impedance spectroscopy (EIS) is a powerful tool for characterizing the interfacial charge transfer process in QDSSCs. The EIS Nyquist plots for the QDSSCs based on TiO_2/CdSe(TDPA), TiO_2/CdSe(MPA), and TiO_2-nano-SiO_2/CdSe(MPA) were shown in Fig. 9. The EIS Nyquist plots exhibited two characteristic peaks. The electrochemical analysis reveals interfacial charge transfer resistance between the Pt counter electrode and electrolyte (R1), interfacial charge transfer resistance among oxide/QDs/electrolyte interface (R2), which were known as Warburg diffusion [34, 35]. As shown in Fig. 9, R1 of the TiO_2/CdSe(TDPA) was bigger than that of other systems, indicating hard mass transport through the electrolyte. Thus, the electron composite was very serious [34]. R2 of the TiO_2-nano-SiO_2/CdSe(MPA) was bigger than that of TiO_2/CdSe(MPA), indicating that the probability of electron recombination is smaller, and the performance of cell was better. The result can be ascribed to the fact that the structure of TiO_2-nano-SiO_2 is beneficial for electrolyte penetration and electron transport, and hence leads to a slower recapture of conduction band electrons by S_n^{2-} ions occurring in the recombination process at counter electrode [36].

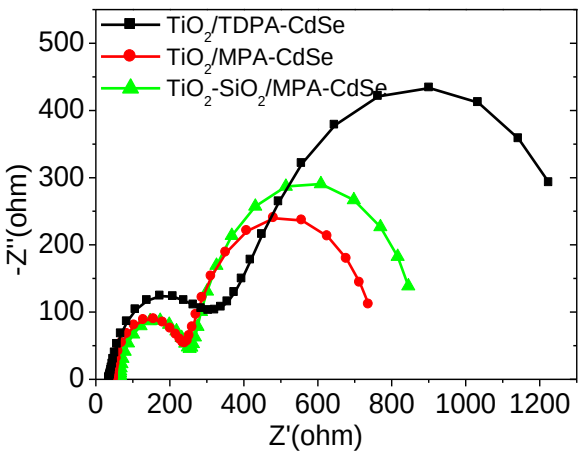

Fig. 9. EIS spectra under the conditions of dark (color online)

4. Conclusion

In summary, we utilize the nano-sized SiO_2 powder and TiO_2 powder as composite materials to fabricate QDSSCs. The photovoltaic performance of QDSSCs is greatly improved by using the ligand exchange and the SiO_2/TiO_2 composite photoanodes. MPA-capped CdSe QDSSCs yields an efficiency of 0.89%, which is higher than that of the TDPA-capped CdSe QDs device (0.45%). The efficiency of a TiO_2-nano-SiO_2/CdSe(MPA) sensitized solar cell is as high as 1.74% under one sun illumination (AM1.5, 100mW/cm^2). Meanwhile, the assembly route of CdSe QDs is green and simple by using the aqueous solvent and the spin-coating method.

Acknowledgements

The work was supported by the Natural Science Foundation of Anhui Province (No.11040606Q45), and the Talent Fund Project of Hefei University (18-19RC41).

References

[1] B. O'Regan, M. Grätzel, Nature **353**, 737 (1991).
[2] N. Nasr, M. H. Sayyad, J. Optoelectron. Adv. M. **20**(11-12), 618 (2018)
[3] Z. Tan, B. Zhao, P. Shen, S. Jiang, P. Jiang, X. Wang, S. Tan, J. Mater. Sci. **46**, 7482 (2011).
[4] Y. Yang, J. Gao, Z. Zhang, S. Xiao, H. H. Xie, Z. B. Sun, J. H. Wang, C. H. Zhou, Y. W. Wang, X. Y. Guo, P. Chu, X. F. Yu, Adv. Mater. **28**, 8937 (2016).
[5] K. Taretto, U. Rau, Prog. Photovoltaics **12**, 573 (2004).
[6] A. J. Nozik, Physica E **14**, 115 (2002).
[7] I. Robel, V. Subramanian, M. Kuno, P. V. Kamat, J. Am. Chem. Soc. **128**, 2385 (2006).
[8] R. D. Schaller, V. I. Klimov, Phys. Rev. Lett. **92**, 186601 (2004).
[9] H. A. Mohamed, M. R. Ahmed, J. Optoelectron. Adv. M. **19**(5-6), 359 (2017)
[10] Z. Y. Gao, N. Liu, D. P. Wu, W. G. Tao, F. Xu, K. Jiang, Appl. Surf. Sci. **258**, 2473 (2012)
[11] R. B. Wang, S. R. Wang, H. H. Niu, S. D. Miao, L. Wan, J. Z. Xu, Optoelectron. Adv. Mat. **8**(1-2), 57 (2014).
[12] T. Shu, Z. M. Zhou, H. Wang, G. H. Liu, P. Xiang, Y. G. Rong, Y. D. Zhao, H. W. Han, J. Nanosci. Nanotechnol. **11**, 9645 (2011).
[13] H. J. Lee, J. H. Yum, H. C. Leventis, S. M. Zakeeruddin, S. A. Haque, P. Chen, S. I. Seok, M. Grätzel, M. K. Nazeeruddin, J. Phys. Chem. C **112**, 11600 (2008).
[14] R. B. Wang, L. Wan, H. H. Niu, Q. Ma, S. D. Miao, J. Z. Xu, J. Sol-Gel Sci. Technol. **67**, 458 (2013).
[15] A. Zaban, O. I. Micic, B. A. Gregg, A. J. Nozik, Langmuir **14**, 3153 (1998)
[16] P. Yu, K. Zhu, A. G. Norman, S. Ferrere, A. J. Frank, A. J. Nozik, J. Phys. Chem. B **110**, 25451 (2006).
[17] L. M. Peter, K. G. U. Wijayantha, D. J. Riley, J. P. Waggett, J. Phys. Chem. B **107**, 8378 (2003).
[18] Y. Yang, W. Y. Wang, J. Power Sources **293**, 577 (2015).
[19] J. T. Li, S. K. Cushing, J. Bright, F. K. Meng, T. R. Senty, P. Zheng, A. D. Bristow, N. Q. Wu, ACS Catal. **3**, 47 (2013).
[20] F. K. Meng, J. T. Li, Z. L. Hong, M. J. Zhi, A. Sakla, C. C. Xiang, N. Q. Wu, Catal. Today **199**, 48 (2013).
[21] F. K. Meng, J. T. Li, S. K. Cushing, J. Bright, M. J. Zhi, J. D. Rowley, Z. L. Hong, A. Manivannan, A. D. Bristow, N. Q. Wu, ACS Catal. **3**, 746 (2013).
[22] J. T. Li, F. K. Meng, S. Suri, W. Q. Ding, F. Q. Huang, N. Q. Wu, Chem Commun **48**, 8213 (2012).
[23] S. Ito, P. Chen, P. Comte, M. K. Nazeeruddin, P. Liska, P. Péchy, M. Grätzel, Prog. Photovolt. Res. Appl. **15**, 603 (2007).
[24] Z. A. Peng, X. G. Peng, J. Am. Chem. Soc. **123**, 183 (2001).
[25] I. Mora-Sero, S. Gimenez, F. Fabregat-Santiago, R. Gomez, Q. Shen, T. Toyoda, J. Bisquert, Acc. Chem. Res. **42**, 1848 (2009).
[26] Y. Lee, C. Chang, J. Power Sources **185**, 584 (2008).
[27] C. Zhang, S. Chen, L. Mo, Y. Huang, H. Tian, L. Hu, Z. Huo, S. Dai, F. Kong, X. Pan, J. Phys. Chem. C **115**, 16418 (2011).
[28] C. He, B. Tian, J. Zhang, J. Colloid. Interf. Sci. **344**, 382 (2010).
[29] K. Zhu, N. R. Neale, A. Miedaner, A. J. Frank, Nano Let. **7**, 69 (2007).
[30] Y. Chen, E. Stathatosb, D. D. Dionysiou, Surf. Coat. Tech. **202**, 1944 (2008).
[31] N. Alexaki, T. Stergiopoulos, A. G. Kontos, D. S. Tsoukleris, A. P. Katsoulidis, P. J. Pomonis, D. J. LeClere, P. Skeldon, G. E. Thompson, P. Falaras, Micropor. Mesopor. Mat. **124**, 52 (2009).
[32] W. W. Yu, X. G. Peng, Angew Chem. Int. Ed. **41**, 2368 (2002).
[33] W. W. Yu, L. Qu, W. Guo, X. G. Peng, Chem. Mater. **15**, 2854 (2003).
[34] W. S. Chi, D. K. Roh, S. J. Kim, S. Y. Heo, J. H. Kim, Nanoscale **5**, 5341 (2013).
[35] Z. Li, Y. Zhou, T. Yu, J. Liu, Z. Zou, Cryst. Eng. Comm. **14**, 6462 (2012).
[36] W. Q. Wu, Y. F. Xu, H. S. Rao, C. Y. Su, D. B. Kuang, Nanoscale **5**, 4362 (2013).

*Corresponding author: rbwang1979@126.com